Bioactive Materials 6 (2021) 219–229

Contents lists available at ScienceDirect

Bioactive Materials

journal homepage: http://www.keaipublishing.com/biomat

# Additive-lathe 3D bioprinting of bilayered nerve conduits incorporated with supportive cells

Jingyi Liu[a,b,1], Bin Zhang[a,1], Liang Li[c], Jun Yin[a,b,*], Jianzhong Fu[a,b]

[a] The State Key Laboratory of Fluid Power and Mechatronic Systems, School of Mechanical Engineering, Zhejiang University, Hangzhou, 310028, China
[b] Key Laboratory of 3D Printing Process and Equipment of Zhejiang Province, School of Mechanical Engineering, Zhejiang University, Hangzhou, 310028, China
[c] Department of Orthopedics, No. 906 Hospital of People's Liberation Army, Ningbo, 315040, China

ARTICLE INFO

*Keywords:*
Nerve conduit
Mesenchymal stem cells
Additive-lathe 3D bioprinting
Gelatin methacrylate
Neuron outgrowth

ABSTRACT

Nerve conduits have been identified as one of the most promising treatments for peripheral nerve injuries, yet it remains unsolved how to develop ideal nerve conduits with both appropriate biological and mechanical properties. Existing nerve conduits must make trade-offs between mechanical strength and biocompatibility. Here, we propose a multi-nozzle additive-lathe 3D bioprinting technology to fabricate a bilayered nerve conduit. The materials for printing consisted of gelatin methacrylate (GelMA)-based inner layer, which was cellularized with bone marrow mesenchymal stem cells (BMSCs) and GelMA/poly(ethylene glycol) diacrylate (PEGDA)-based outer layer. The high viability and extensive morphological spreading of BMSCs encapsulated in the inner layer was achieved by adjusting the degree of methacryloyl substitution and the concentration of GelMA. Strong mechanical performance of the outer layer was obtained by the addition of PEGDA. The performance of the bilayered nerve conduits was assessed using *in vitro* culture of PC12 cells. The cell density of PC12 cells attached to cellularized bilayered nerve conduits was more than 4 times of that on acellular bilayered nerve conduits. The proliferation rate of PC12 cells attached to cellularized bilayered nerve conduits was over 9 times higher than that on acellular bilayered nerve conduits. These results demonstrate the additive-lathe 3D bioprinting of BMSCs embedded bilayered nerve conduits holds great potential in facilitating peripheral nerve repair.

## 1. Introduction

Injuries to peripheral nerves are one of the most common forms of trauma. These injuries affect the life quality of patients and lead to a large number of disabilities. Peripheral nerves exhibit self-healing potential after mild and moderate trauma. However, successful re-innervation cannot always be achieved, especially in the scenario of wide injury gap, e.g. > 5 mm [1,2]. Current clinical strategies, including nerve coaptation and autografts, are restricted by donor site morbidity, limited graft availability, and large gap length [3,4]. As an alternative, nerve conduits, tubular scaffolds to fill the larger gap, exhibit promising results for facilitating peripheral nerve defect repair [5–7]. Nerve conduits maintain adequate mechanical support for the regenerating nerves and create an optimal microenvironment for the proliferation and maturation of Schwann cells and the regeneration of axons [2]. Nerve conduits show promise for clinical application, since they are easy to fabricate and sterilize and simple to implant in the body.

The ideal nerve conduit must satisfy several biological and physicochemical requirements. First, the nerve conduits should have good biocompatibility and have no toxic side effect on the surrounding tissues during in *vivo* implantation [8]. These features allow the nerve conduit to serve as a substrate that supports appropriate cellular behaviors of regenerating nerves. Second, the nerve conduit should be sufficiently physically robust to resist *in vivo* physiological invasion, avoid channel collapse, and mechanically match the nerve tissues [9]. Although, various natural and synthetic materials have been utilized to develop the nerve conduits, the nerve injury repair efficiency of existing nerve conduits is still unsatisfactory due to their inappropriate biological and mechanical properties or lack of structural integration. For example, chitosan conduits with a laminin-coated inner surface are considered to have good biocompatibility, but the mechanical strength

Peer review under responsibility of KeAi Communications Co., Ltd.
* Corresponding author. The State Key Laboratory of Fluid Power and Mechatronic Systems, School of Mechanical Engineering, Zhejiang University, Hangzhou, 310028, China.
*E-mail address:* junyin@zju.edu.cn (J. Yin).
[1] Jingyi Liu, and Bin Zhang contributed equally to this work.

https://doi.org/10.1016/j.bioactmat.2020.08.010
Received 28 May 2020; Received in revised form 29 July 2020; Accepted 11 August 2020

of chitosan conduits was too weak for clinical application [10]. In contrast, polycaprolactone (PCL) fumarate-based conduits were found to be sufficiently mechanically strong, but cell attachment on PCL conduits was found to be inhibited [11]. Thus, single-layered nerve conduits are subjected to trade-offs between mechanical strength and biocompatibility. As a result, bilayer nerve conduits were developed to improve both biocompatibility and mechanical properties. However, previous studies showed the inner layer of bilayered nerve conduits tended to detach from the outer layer, i.e. laminin-coated chitosan/silicone tube [10]. But, the soft inner laminin-coated chitosan layer easily collapsed and blocked the conduit lumen, which severely impaired the regeneration of neurons. Therefore, the fabrication of fully integrated bilayered nerve conduits was explored to avoid potential risks of insufficient nerve growth, discontinuities and structural weakness.

In the pursuit of an effective nerve conduit many biological strategies, including stem cell therapy [12,13], have been employed during fabrication. Bone marrow mesenchymal stem cells (BMSCs), multipotent cells with the ability to differentiate into many lineages including neural-like lineages, were repeatedly found to support nerve regeneration [10,14–16]. However, cell seeding protocols typically involve either cell attachment in culture after fabrication, which potentially results in cell detachment *in vivo*, or cell lumen injection, which is susceptible to leakage [17]. Furthermore, these cell seeding methods do not allow for precise control of cell number or cellular distribution within the nerve conduits [18]. To overcome these challenges, 3D bioprinting with cell-laden bioinks provides a promising method to embed living cells into structures during fabrication. This technique allows not only control of spatial distribution and cell density but also customization with a specified diameter and complex architectures.

Here we developed a multi-nozzle additive-lathe 3D bioprinting method to manufacture fully integrated bilayered nerve conduit incorporating BMSCs. The nerve conduit consisted of a gelatin methacrylate (GelMA)-based inner layer and a GelMA/poly(ethylene glycol) diacrylate (PEGDA)-based outer layer. While the inner layer was greatly biocompatible to provide an appropriate microenvironment for nerve regeneration, the mechanical properties of the outer layer were strong enough for structural support. The biocompatibility and mechanical properties of GelMA with/without PEGDA hydrogels were characterized through *in vitro* cellular and mechanical tests, respectively. Prior to 3D bioprinting of bilayered nerve conduits, the influence of the degree of methacryloyl substitution (DMS) and the concentration of GelMA on the viability and morphology of embedded BMSCs were carefully characterized for inner layer material selection. Subsequently, the microstructure and mechanical strength of the resulting nerve conduits were examined by scanning electron microscopy (SEM) and compression tests, respectively. Finally, the morphology and proliferation of neuron-like PC12 cells seeded on the printed nerve conduits were analyzed by immunofluorescent staining and CCK-8 tests for the potential applications of the nerve conduit in nerve tissue regeneration. This study provided a promising method for the manufacturing of bilayered nerve conduits with supportive cells for peripheral nerve regeneration.

## 2. Materials and methods

### 2.1. Materials

Gelatin obtained from porcine skin tissue (250 bloom, Type B) and methacrylic anhydride (MA) were purchased from Aladdin Industrial (China). PEGDA ($Mn$ = 700) was purchased from Sigma-Aldrich (USA). The photoinitiator, lithium phenyl-2,4,6-trimenthylbenzoyphosphinate (LAP), was synthesized as previously described [19]. Dulbecco's Modified Eagle Medium (DMEM) was purchased from HyClone Laboratories Inc. (Canada). The Live/Dead Viability Assay Kit and Cell Counting Kit-8 (CCK-8) were bought from Beyotime Biotechnology (China). 4′,6-diamidino-2-phenylindole (DAPI) and phalloidin-FITC were obtained from Beijing Solarbio Science & Technology Co., Ltd (China). PC12 cells and murine BMSCs were obtained from the Chinese Academy of Sciences (Shanghai, China).

### 2.2. Synthesis of GelMA and proton nuclear magnetic resonance characterization

Gelatin methacrylate (GelMA) was synthesized as previously described [20,21]. Briefly, gelatin was dissolved in carbonate-bicarbonate buffer at 50 °C under continuous stirring and MA was added. Different volumes of MA were added into gelatin solution (MA/gelatin feed ratio: 0.0125/1, 0.025/1, 0.05/1, and 0.1/1 mL/g) for the synthesis of GelMA with various DMS. After reaction in dark for 3 h, the products were diluted with 5-fold phosphate buffer saline (PBS) and then dialyzed against distilled water for 7 days at 40 °C. The products were then filtered with 0.22 μm paper filter and lyophilized, leading to a white porous foam, before being stored at −20 °C for further use.

The DMS, the percentage of ε-amino groups in gelatin replaced by methacryloyl groups, of GelMA was quantified by the proton nuclear magnetic resonance ($^1$HNMR, Bruker Avance 400, Switzerland) according to previously reported methods [22,23]. GelMA/gelatin was dissolved in deuterium oxide at 40 mg/mL at 40 °C, and the spectra were obtained at 40 °C. The peak area of aromatic acids (6.9–7.5 ppm) in the GelMA or gelatin samples was used as a reference in each spectrum. The peak area of lysine methylene (2.8–2.95 ppm) was used for the calculation of the DMS as:

$$\text{DMS}\ (\%) = \left(1 - \frac{\textit{Area of lysine methylene in GelMA}}{\textit{Area of lysine methylene in gelatin}}\right) \times 100 \quad (1)$$

### 2.3. Preparation of GelMA/PEGDA precursor solutions

GelMA precursor solutions with different values of GelMA concentration (5%, 10%, 15%, 20%, and 30%, w/v) and DMS (MA/gelatin: 0.0125/1, 0.025/1, 0.05/1, and 0.1/1 mL/g) were prepared by dissolving freeze-dried GelMA in PBS carrying 0.5% (w/v) LAP at 50 °C. As for GelMA/PEGDA precursor solutions, different volumes of PEGDA were added into the abovementioned GelMA precursor solutions (PEGDA:GelMA = 1:9, 3:17, 1:4, and 1:3 v/v). The concentration of photoinitiator (LAP) was also 0.5% (w/v) for GelMA/PEGDA precursor solutions.

### 2.4. Culture of BMSCs in GelMA hydrogels

BMSCs were embedded in nerve conduits as supportive cells. BMSCs were cultured in DMEM supplemented with 10% (v/v) fetal bovine serum (FBS, Beyotime Biotechnology Co., Ltd, China) and 1% (v/v) penicillin-streptomycin (PS, Shanghai Macklin Biochemical Co., Ltd, China). The culture was maintained in a humidified incubator (Thermo Fisher Scientific, USA) at 37 °C with 5% $CO_2$. At 80% confluence, BMSCs were dissociated using 0.25% trypsin and then incorporated into the GelMA precursor solutions to obtain cell suspensions with a cell density of $1 \times 10^6$ cells/mL.

To investigate BMSC viability and cell circularity in GelMA hydrogels, 300 μL aliquots of cell suspension were transferred into polylactic acid molds (inner diameter: 10 mm). The cell suspension was then photocrosslinked under UV light (365 nm, 2W/cm$^2$) at a distance of 1 cm for 2 min, forming a GelMA hydrogel cylinder (diameter: 10 mm, height: 3.8 mm) with embedded BMSCs. The hydrogel cylinders were transferred into tissue culture dishes and DMEM [10% (v/v) FBS, 1% (v/v) PS] was added and maintained under humid conditions at 37 °C with 5% $CO_2$. After 24, 72, and 120 h of cell culture, the viability and circularity of BMSCs incorporated into the GelMA cylinder were assessed by a live/dead assay. Live cells were stained with calcein-AM and dead cells with propidium iodide (PI). The stained hydrogel samples

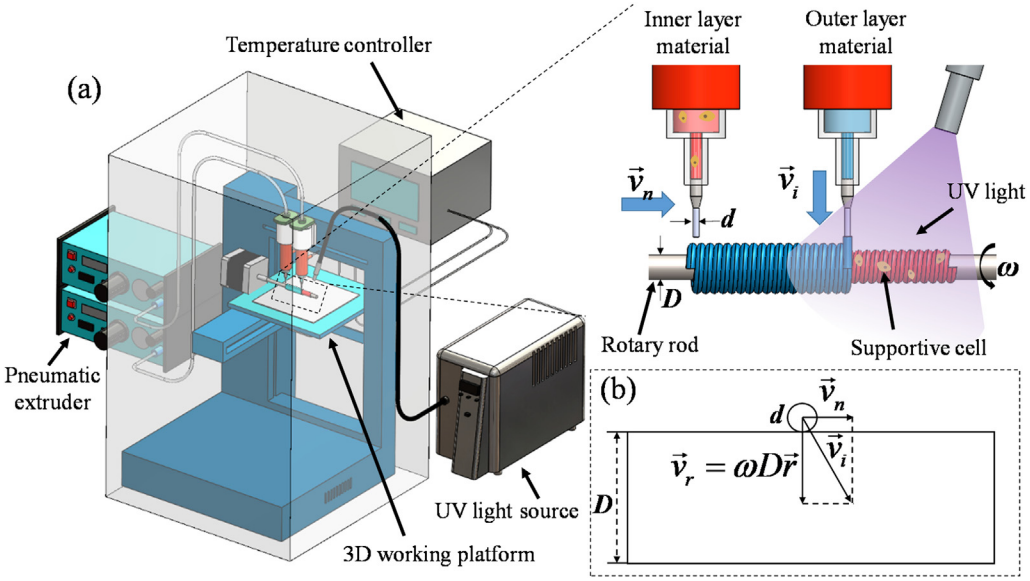


**Fig. 1.** (a) Schematic of the additive-lathe 3D bioprinting setup used to fabricate bilayered nerve conduits. (b) Synchronization of nozzle speed, bioink flow speed, and rotating rod speed.

were imaged using an inverted phase-contrast fluorescence microscope (Nikon Ti–U, Japan). The obtained images were analyzed using the ImageJ software (Version 1.52a, National Institutes of Health).

To investigate the morphology of BMSCs encapsulated in GelMA hydrogels, BMSCs were immunofluorescently stained after 0, 5, 14, and 21 days of culture. BMSCs embedded in GelMA hydrogel cylinders were fixed in 4% paraformaldehyde (Shanghai Macklin Biochemical Co., Ltd, China), and permeabilized with Triton X-100 (Shanghai Macklin Biochemical Co., Ltd, China). Then, the phalloidin-FITC stain was added to the GelMA hydrogel cylinders at room temperature in darkness. Next, cell nuclei were stained using DAPI dye. Finally, the stained samples were washed three times with PBS and imaged using confocal microscopy (Olympus FV1000 BX61, Japan).

### 2.5. Mechanical testing of GelMA/PEGDA hydrogels

A commercial testing machine, ElectroForce (TA Instruments, USA), was utilized to determine the mechanical properties of GelMA/PEGDA hydrogels. For unconfined compression tests, 300 μL GelMA or GelMA/PEGDA precursor solution was filled into plastic molds (inner diameter: 10 mm) and exposed to UV light (365 nm, 2 W/cm$^2$) at a distance of 1 cm for 2 min. Each hydrogel sample was compressed at a displacement rate of 1 mm/min. Stripes of GelMA/PEGDA hydrogels (4 mm × 4 mm × 28 mm) were stretched at a displacement rate of 1 mm/min to explore the tensile properties. The compressive and Young's modulus were determined based on the slope of the linear region in the 0%–10% strain range of the stress-strain curves.

### 2.6. Enzymatic degradation and water content of GelMA/PEGDA hydrogels

A collagenase degradation assay was carried out to evaluate the degradation of GelMA hydrogels with different DMS and concentrations as described before [24]. Briefly, GelMA hydrogel samples with a diameter of 10 mm and thickness of 2 mm were fabricated. After being placed in PBS for 24 h to reach the equilibrium swelling, GelMA hydrogel samples were incubated into the enzyme solution containing 2.5 U/mL collagenase and 0.5 mM CaCl2 at 37 °C [25]. The biodegradation of GelMA hydrogels was indicated by the percentage of remaining weight of the samples after degradation as [21]:

$$Q_d = \frac{W_r}{W_s} \times 100\% \quad (2)$$

where $W_s$ denotes the swollen weight of samples and $Wr$ the remaining weight, respectively.

The water content of GelMA/PEGDA hydrogels was determined by measuring the weight change upon water absorption. GelMA/PEGDA hydrogels were immersed in PBS and maintained at 37 °C under magnetic stirring overnight. The samples were weighed after removing excess water using filter paper. Water content was determined as:

$$\text{Water content} = \frac{W_s - W_d}{W_s}, \quad (3)$$

where $W_s$ and $W_d$ represent the swelling weight and dry weight of hydrogel samples, respectively.

### 2.7. Rheological testing of GelMA/PEGDA hydrogels

The rheological behaviors of nerve conduit materials were analyzed using an MCR 102 rheometer (Anton Paar, Austria). A plate-plate geometry with a diameter of 25 mm was used in all measurements. The rotational shear-viscosity measurements were performed in flow mode with shear rates between 0.05 and 500 s$^{-1}$ at 25 °C. The linear viscoelastic region (LVER) was measured at a controlled shear strain increasing from 1 to 100% with amplitude sweeps at 10 rad/s. The dynamic frequency sweep tests at 1–100 rad/s were performed with a constant shear strain of 10% to determine the storage ($G'$) and loss ($G''$) moduli of nerve conduit materials within the LVER. Subsequently, the influence of temperature (10–40 °C) on $G'$ and $G''$ were measured at a constant angular frequency of 10 rad/s and a constant strain of 1%. To assess the kinetics of the photocrosslinking reaction of GelMA/PEGDA (irradiated with 365 nm UV), time sweeps were performed with the same angular frequency and strain setting as temperature sweeps [26].

### 2.8. Bioprinting of bilayered nerve conduits

Bilayered nerve conduits were printed using the additive-lathe 3D bioprinting technology, as has been described previously [27]. All nerve conduits were fabricated using a multi-nozzle 3D pneumatic dispensing system comprised of a computer-controlled three-axis positioning stage, controllable pneumatic extruder, temperature controller, UV light source, and a rotary device (Fig. 1a). First, the inner layer of the nerve conduit was formed by the extrusion of GelMA with/without BMSCs, and the resulting filament was reeled over a rotating rod. Then,

**Table 1**
Groups of printed nerve conduits.

| Nerve conduit group | Materials | |
|---|---|---|
| | Inner layer | Outer layer |
| Stiff single-layered nerve conduit | Same as outer layer | 30% (w/v) GelMA (MA/gelatin: 0.1/1 mL/g), 20% (v/v) PEGDA |
| Soft single-layered nerve conduit | 5% (w/v) GelMA (MA/gelatin: 0.05/1 mL/g) | Same as inner layer |
| Acellular bilayered nerve conduit | 5% (w/v) GelMA (MA/gelatin: 0.05/1 mL/g) | 30% (w/v) GelMA (MA/gelatin: 0.1/1 mL/g), 20% (v/v) PEGDA |
| Cellularized bilayered nerve conduit | BMSCs embedded, 5% (w/v) GelMA (MA/gelatin: 0.05/1 mL/g) | 30% (w/v) GelMA (MA/gelatin: 0.1/1 mL/g), 20% (v/v) PEGDA |

the GelMA/PEGDA was deposited onto the inner layer generating a bilayered spiral nerve conduit. A Live/Dead assay was used to assess the cell viability of BMSCs in nerve conduits immediately after printing. Throughout the printing process, the nozzle was constrained to the horizontal movement and the rod was maintained at rotational movements to control filament deposition at precisely defined locations allowing the fusion of adjacent filaments. A two-step crosslinking strategy was implemented during printing to ensure sufficient interfacial strength between the two layers of the nerve conduit [20]. In the first step, GelMA/PEGDA precursor solutions underwent thermo-crosslinking by adjusting the syringe temperature controller between 14 and 26 °C to form stable filaments. Meanwhile, the deposited filaments were exposed under UV light (365 nm, 0.5 W/cm$^2$) at a distance of 1 cm allowing photocrosslinking of GelMA/PEGDA. In the second step, the printed bilayered nerve conduits were exposed to UV light (365 nm, 2 W/cm$^2$) at a distance of 1 cm for an additional minute to ensure permanent structural integrity. The soft and stiff single-layered nerve conduits were manufactured through the same method. All the groups of printed nerve conduits are listed in Table 1.

To avoid the dispersion or accumulation of printed filaments, the synchronization was conducted as (Fig. 1b):

$$\vec{V_i} = \vec{V_n} + \vec{V_r}, \tag{4}$$

and it can be geometrically obtained that [28]:

$$\vec{V_n} = \frac{d}{2\pi}\omega \text{ and } \vec{V_l} = \frac{\sqrt{d^2 + \pi^2(D+d)^2}}{2\pi}\omega, \tag{5}$$

where $\vec{V_n}$, $\vec{V_i}$, and $\vec{V_r} = \omega D\vec{r}$ denote nozzle speed, bioink flow speed, and rotating rod speed, respectively. $D$, $d$ and $\omega$ are rod diameter, nozzle outlet diameter and angular speed of rotating rod, respectively. The operation parameters of the additive-lathe 3D bioprinting are listed in Table 2.

### 2.9. Mechanical tests of nerve conduits

The mechanical properties of nerve conduits (both single-layered and bilayered) were measured by an ElectroForce (TA Instruments, USA) at room temperature. The compressive modulus of nerve conduits was measured by lateral compression at a rate of 1 mm/min [9,29]. The compressive modulus was defined as:

$$A_0 = \lim_{\varepsilon \to 0} \frac{F}{\varepsilon}, \tag{6}$$

**Table 2**
Parameters of additive-lathe 3D bioprinting.

| Parameters | Value |
|---|---|
| Nozzle temperature of inner layer material | 14 °C |
| Extrusion pressure of inner layer material | 0.08–0.12 MPa |
| Nozzle temperature of outer layer material | 26 °C |
| Extrusion pressure of outer layer material | 0.18–0.22 MPa |
| Rod rotating angular velocity | 1–5 rad/s |
| Velocity of the printing nozzle | 0.1–4 mm/s |
| Outlet diameter of printing nozzle | 0.5 mm |
| Diameter of the rotating rod | 1.6 mm |

where $F$ was the compressive force per unit length and $\varepsilon = (OD - OD')/OD$ is the compressive strain. Here, $OD$ and $OD'$ represent the outer diameter before and after compression, respectively.

### 2.10. PC12 cells cultured on nerve conduits

Since the culture of PC12 cells has been reported as suitable models for the study of the biomedical and functional properties of neuronal cells *in vitro* [7], PC12 cells were adopted to characterize the neuron regeneration on nerve conduits. Here, PC12 cells were cultured in DMEM supplemented with 5% FBS and 1% PS. When the cells reached a confluence of 90% PC12 cells were seeded onto the inner surface of four nerve conduits (Table 1) with a density of $1.5 \times 10^5$ cells per nerve conduit. The nerve conduits seeded with PC12 cells were then placed inside an incubator at 37 °C in 5% $CO_2$. After 1 and 3 days of culture, PC12 cells were stained with DAPI and phalloidin-FITC and observed using a confocal microscope. These fluorescence images were analyzed using FV-1000 software for cell morphology and ImageJ software for counting numbers of PC12 cells adhered to nerve conduits.

The proliferation of PC12 cells was evaluated based on a CCK-8 cell counting assay according to the manufacturer's instructions. PC12 cells were seeded onto nerve conduits (with/without BMSCs) with a density of $5 \times 10^3$ cells per nerve conduit. The nerve conduits were then placed in 96-well plates. After 1 and 3 days of incubation, CCK-8 solution was added into the culture medium of each well at a volume ratio of 1:10 of CCK-8 solution to medium. Then, cell cultures were returned to the incubator for 2 h. Subsequently, the absorbance of the culture medium of PC12 cells on nerve conduits was measured by a microplate reader (BioTex, USA) at 450 nm.

### 2.11. Scanning electron microscope observation

SEM (TM-100; HITACHI, Japan) was used to analyze the structural characteristics of the generated bilayered nerve conduits without BMSCs. Before scanning, samples were frozen and dried in a vacuum freeze-drying machine (DYYB-10; Shanghai Deyangyibang Instruments Co., Ltd., China) for 24 h and sputter-coated with gold for 10 min. The porosity and pore size of the bilayered nerve conduit were determined using ImageJ software [30].

### 2.12. Statistics

Unless otherwise stated, all characterizations were performed using data analysis software OriginPro 2017 (OriginLab). Mean values and standard deviation values were calculated for all quantitative measures. The statistical significance of experimental data was calculated using the one-way analysis of variance, and significance was determined at $p < 0.05$.

## 3. Results

### 3.1. DMS of GelMA hydrogels

In this work, the DMS of GelMA was regulated by changing MA/gelatin feed ratio during GelMA synthesis. As shown in Fig. 2, four

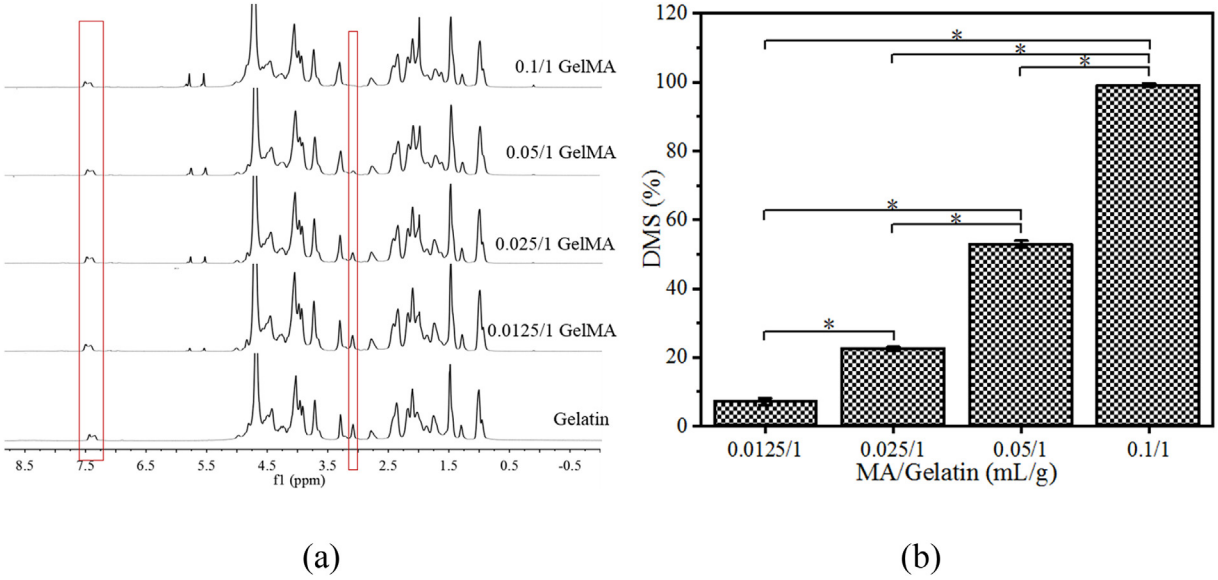


**Fig. 2.** (a) $^{1}$HNMR spectra of unmodified gelatin and GelMA with different DMS. The left and right boxes represent the signals of aromatic amino acid and lysine amino acid, respectively. (b) The relationship between DMS of GelMA and MA/gelatin feed ratio.

different MA (mL)/gelatin (g) feed ratios (0.1/1, 0.05/1, 0.025/1, and 0.0125/1) were utilized for GelMA synthesis. The decreased signal at $\delta$ = 2.9 ppm confirmed the increase of DMS with the feed ratio of MA to gelatin (Fig. 2a). As defined in Eq. (1), the DMS is found to be approximately proportional to MA/gelatin feed ratio. At a MA/gelatin feed ratio of 0.1/1 (mL/g) the reaction reached almost complete methacryloylation of ε-amino groups, where DMS was 99.2 ± 0.42. (Fig. 2b). The DMS values of GelMA with MA/gelatin feed ratio of 0.05/1, 0.025/1, and 0.0125/1 were 52.86 ± 1.01, 22.5 ± 0.51, and 7.14 ± 1.02, respectively (Fig. 2b).

### 3.2. Mechanical and degradative properties of GelMA/PEGDA hydrogels

Higher DMS and concentration of GelMA lead to a significant increase in GelMA hydrogels' Young's and compressive modulus (Fig. 3a and b). The 0.1/1 30% (w/v) GelMA hydrogel had the highest Young's modulus (318.46 ± 29.26 KPa) and compressive modulus (304.15 ± 44.88 KPa), which was almost 300 times higher than those of 0.025/1 10% (w/v) GelMA (Young's modulus: 1.27 ± 0.22 KPa; compressive modulus: 2.18 ± 1.14 KPa). Thus, the mechanical properties of GelMA hydrogel can be effectively regulated by adjusting the DMS and concentration of GelMA.

The addition of PEGDA significantly enhanced the mechanical properties of GelMA hydrogels for further clinical application. PEGDA was mixed into GelMA to form GelMA/PEGDA composite hydrogel. When PEGDA concentration increased from 0 to 25% (v/v) in 0.1/1 30% (w/v) GelMA hydrogel, Young's modulus and compressive modulus of GelMA/PEGDA hydrogels increased from 0.3 to 2.9 MPa and from 0.3 to 3.4 MPa, respectively (Fig. 3c and d). It demonstrated that the addition of PEGDA significantly enhanced the mechanical properties of GelMA hydrogels.

Fig. 3e shows the degradation rate was highly dependent on the DMS and concentration of GelMA hydrogels, and the higher DMS and concentration of GelMA hydrogels lead to a slower degradation rate. Although, 0.05/1 5% (w/v) GelMA fully degraded within 35 h in the enzyme solution, the *in vivo* degradation rate of GelMA hydrogel is much slower than that in the enzyme solution [31,32]. Thus, the bilayered nerve conduits are appropriate for the *in vivo* application.

### 3.3. BMSCs culture encapsulated in GelMA hydrogels

To understand the influence of GelMA's DMS and concentration on encapsulated cells, the viability, circularity, and morphology of BMSCs were characterized by Live/Dead Viability Assay and DAPI/phalloidin-FITC staining. Live/dead cell staining after 1, 3, and 5 days of culturing indicated that BMSCs viability decreased with the DMS and concentration of GelMA hydrogels (Fig. 4a). DAPI/phalloidin-FITC staining revealed that BMSCs encapsulated inside 0.05/1 5% (w/v) GelMA hydrogel had more extensive morphology than in other GelMA hydrogels (Fig. 4b). Statistical cell viability analysis exhibited the same trend that BMSCs had the highest cell viability (> 95%) when they were embedded in 0.05/1 5% (w/v) GelMA hydrogel (Fig. 4c) during 5 days of culture. BMSCs cultured in 0.05/1 5% (w/v) GelMA hydrogel have the lowest circularity at 0.63 ± 0.14, while those in other groups have the circularity of large than 0.9 after 5 days of culture, indicating 0.05/1 5% (w/v) GelMA hydrogel has the best biocompatibility for BMSC culture (Fig. 4d).

The morphology of BMSCs embedded in 0.05/1 5% (w/v) GelMA hydrogel during a long term *in vitro* culture is shown in Fig. 5. It can be found that F-actin in BMSCs stretched after cell culture of 5 days, and BMSCs extensively spread with abundant F-actin filaments and formed a network after cell culture of 21 days. Therefore, 0.05/1 5% (w/v) GelMA hydrogel was demonstrated to have excellent biocompatibility for BMSCs culture.

### 3.4. Material selection for bilayered nerve conduits

Based on the mechanical properties of GelMA/PEGDA hydrogels (Fig. 3c and d), 0.1/1 30% (w/v) GelMA/20% (v/v) PEGDA was sufficiently mechanically strong for clinical operation [33,34]; thus, 0.1/1 30% (w/v) GelMA/20% (v/v) PEGDA was selected as the outer layer material of nerve conduits. It is noted that 0.1/1 30% (w/v) GelMA/25% (v/v) PEGDA had poor processability because GelMA extrusion with more than 20% (v/v) PEGDA leads to uneven filaments. In light of the results of BMSCs culture encapsulated in GelMA hydrogels (Figs. 4 and 5), 0.05/1 5% (w/v) GelMA was chosen as inner layer material of nerve conduit, due to its high cell viability and best cell morphology.

To fabricate the bilayered nerve conduits by additive-lathe 3D bioprinting (Fig. 1), the printability of the inner (0.05/1 5% (w/v) GelMA) and outer (0.1/1 30% (w/v) GelMA/20% (v/v) PEGDA) layer

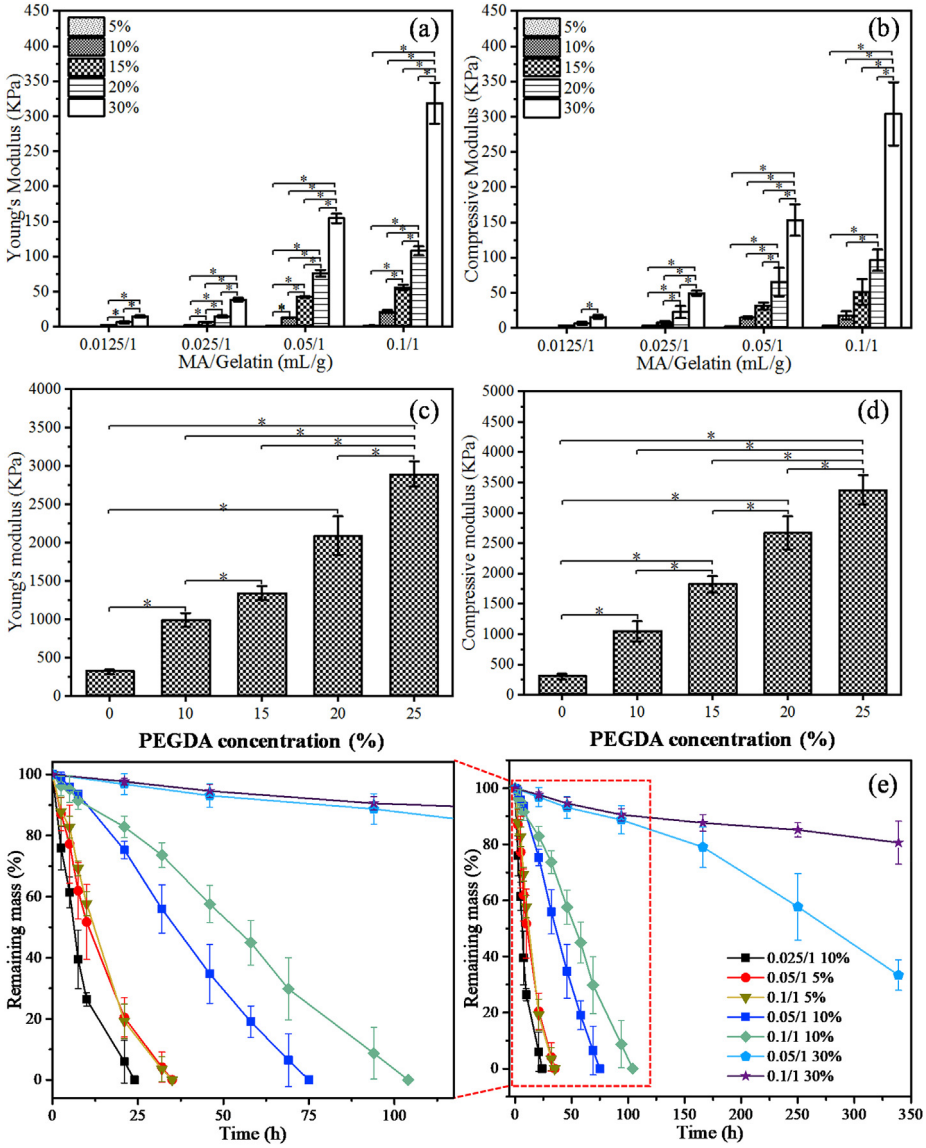


**Fig. 3.** Young's modulus (a), compressive modulus (b) of GelMA hydrogels with different DMS and concentrations. Young's modulus (c) and compressive modulus (d) of 0.1/1 30% (w/v) GelMA with PEGDA of different concentrations. (e) Enzymatic degradation profiles of GelMA hydrogels with different DMS and concentrations.

materials was assessed through rheological tests. As shown in Fig. 6a, both inner and outer layer hydrogels (Table 1) exhibited a shear-thinning behavior which is critical for extrusion-based printing. Additionally, the viscosity of outer layer hydrogel was much greater than that of the inner layer hydrogel. The results of oscillatory shear tests demonstrated that the inner layer hydrogel exhibited liquid-like behavior ($G'' > G'$) across all frequencies, while the outer layer hydrogel showed solid-like behavior ($G' > G''$) in the oscillation frequency sweep (Fig. 6b). The hydrogels' shear moduli ($G'$ and $G''$) are temperature-dependent (Fig. 6c). Prior to gelation, both pure GelMA and GelMA/PEGDA hydrogels showed a typical fluid-like behavior ($G'' > G'$). The storage modulus ($G'$) of both hydrogels increased rapidly and eventually crossed over loss modulus ($G''$) during cooling showing a gel-like characteristic. The gelation temperature ($G' = G''$) for 0.1/1 30% (w/v) GelMA/20% PEGDA was around 26 °C, while 0.05/1 5% GelMA exhibited a lower gelation temperature around 14 °C. Also, the rheological properties of GelMA/PEGDA hydrogels were monitored during the UV-curing process to assess the kinetic of the photocrosslinking reaction. Fig. 6d shows that both inner and outer layer hydrogels became stiffer as UV curing time increased, and finally reached their gelation points ($G' = G''$). The gelation time (when $G' = G''$) of 0.1/1 30% (w/v) GelMA/20% PEGDA (2 s) was much shorter than that of 0.05/1 5% GelMA (54 s).

The water contents (Eq. (3)) of inner and outer layer hydrogels were measured as 17.61 ± 1.03 and 2.51 ± 0.36, respectively. The GelMA inner layer had a much higher water content than outer layer hydrogel. Since a higher water content facilitates the transportation of necessary nutrition for cell outgrowth within the hydrogel, BMSCs culture encapsulated in GelMA inner layer was promoted.

### 3.5. 3D bioprinting of bilayered nerve conduits

A bilayered nerve conduit with an inner diameter of 1.6 mm and length of 15 mm was fabricated (Fig. 7) through additive-lathe 3D bioprinting (Fig. 1). The morphology and geometry of bilayered nerve conduit was observed by SEM. The inner diameter of the fabricated nerve conduits matched with the size of the rotary rod, while the wall thickness of both inner and outer layers was approximately equivalent to the printing nozzle diameter (around 500 μm, Fig. 7c and d). Therefore, the bilayered nerve conduits showed an excellent shape fidelity by optimizing 3D printing conditions (Table 2). The porous morphology of both inner and outer layers was also observed in Fig. 7a

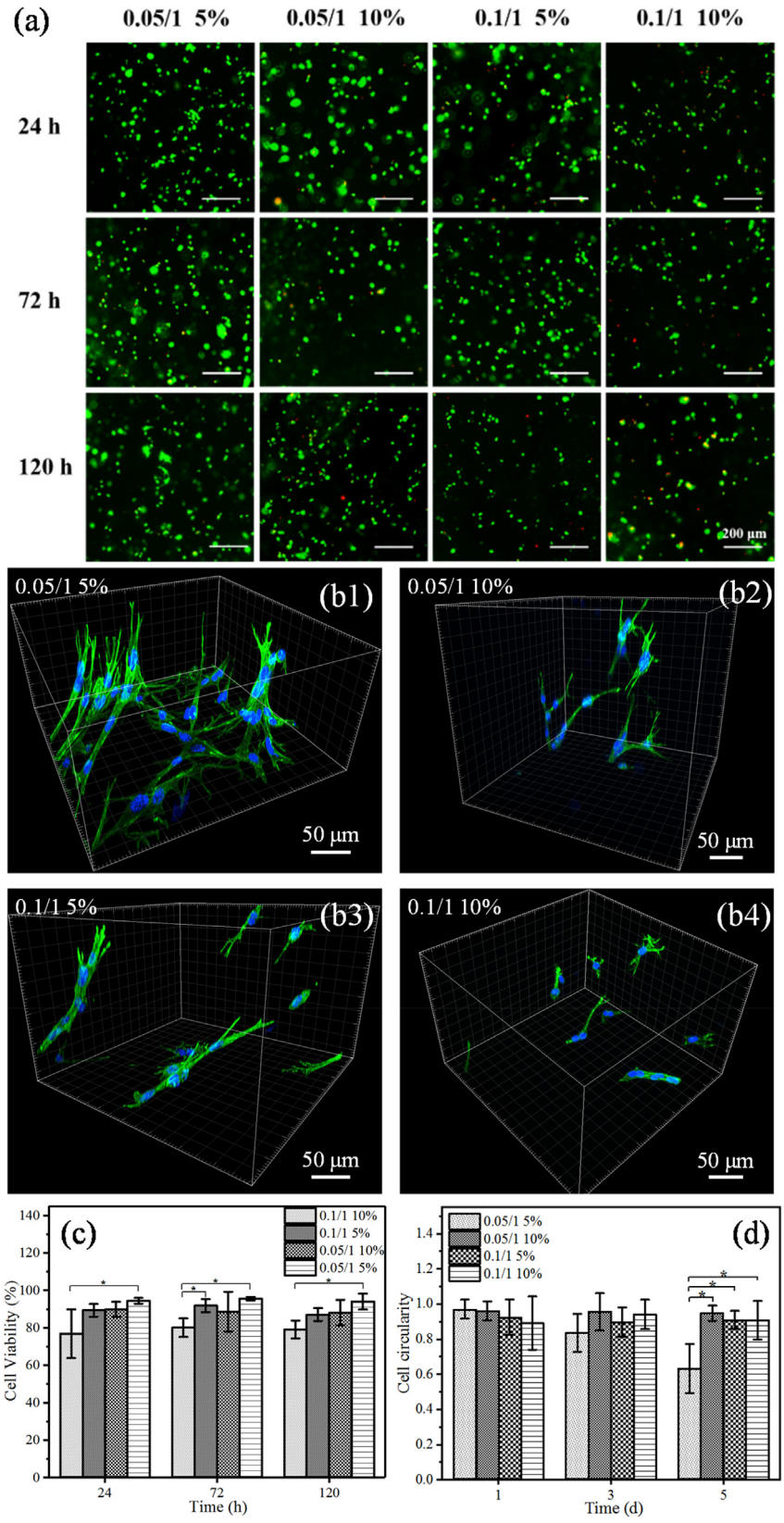


**Fig. 4.** Cell viability, circularity, and morphology of BMSCs encapsulated in GelMA hydrogels with different DMS and concentrations. (a) Live/Dead assay by calcein-AM and PI staining on days 1, 3, and 5. Living cells are depicted in green and dead cells are in red. (Scale bar: 200 μm) (b) Immunofluorescent staining of BMSCs embedded in GelMA after 5 days of culture. (c) Statistical cell viability. (d) Statistical results of cell circularity.

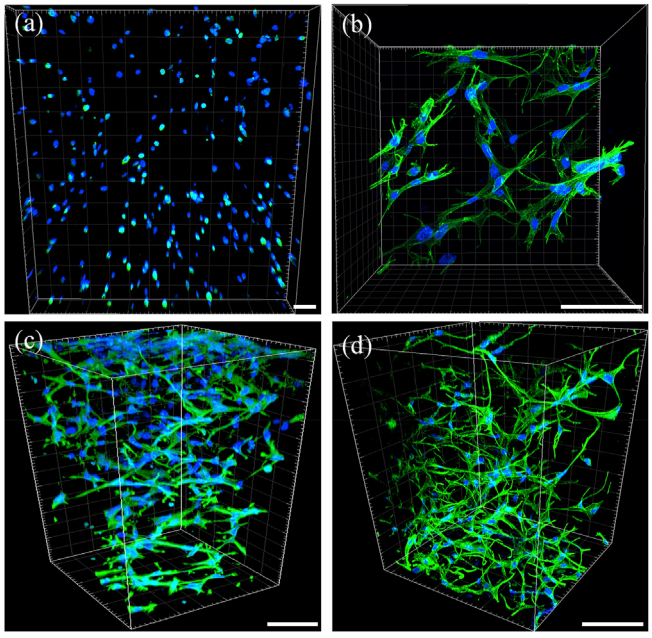


**Fig. 5.** Confocal laser microscopy images of BMSCs stained with F-actin (green) and cell nuclei (blue) after being cultured in 0.05/1 5% (w/v) GelMA hydrogels for 0 day (a), 5 days (b), 14 days (c) and 21 days (d). (Scale bar: 100 μm).

and (b). The inner layer has a higher porosity (53.31 ± 11.51%) and a larger average pore size (41.27 ± 8.08 μm) than that of the outer layer (29.78 ± 3.94% and 14.94 ± 2.84 μm, respectively), which led to larger water content and better cell viability of the inner layer. The deposition of inner and outer layer hydrogels was precisely controlled by synchronization equation (Eq. (5)), and the deposited filaments were further fused with adjacent filaments. The inner layer of printed nerve conduit had the intact lumen, and uniform diameter (Fig. 7h), creating an appropriate microenviorment for peripheral nerve regeneration. Besides, inner and outer layers were found to be seamlessly integrated, which is of great importance to improve the mechanical strength of nerve conduits. Live/Dead staining showed significantly high cell viability in the inner layer of the nerve conduit, indicating that the additive-lathe 3D bioprinting was friendly for living BMSCs during printing, which is the prerequisite for achieving cell function (Fig. 7g and h).

Compression tests were performed to characterize the mechanical properties for both single-layered and bilayered nerve conduits, and it is found that the compressive modulus of both stiff single-layered nerve conduit (2.3 ± 0.38 N/mm) and bilayered nerve conduit (1.61 ± 0.50 N/mm) was significantly higher than that of soft single-layered nerve conduit (0.014 ± 0.005 N/mm). Obviously, the mechanical properties of soft single-layered nerve conduits are enhanced by inducing a 0.1/1 30% (w/v) GelMA/PEGDA hydrogel layer, which is a feasible way to improve the mechanical performance of nerve conduits while keeping good biocompatibility of inner layer. The similar tendency could be observed in cyclic compression and three-point bending tests (Fig. S1).

### 3.6. PC12 cells seeded on nerve conduits

To evaluate the effects of BMSCs on PC12 cell differentiation and proliferation, PC12 cells were cultured on the inner surface of four nerve conduits (Table 1). Before bioprinting of nerve conduits, different cell trackers were used to fluorescently label BMSCs and PC12 cells for

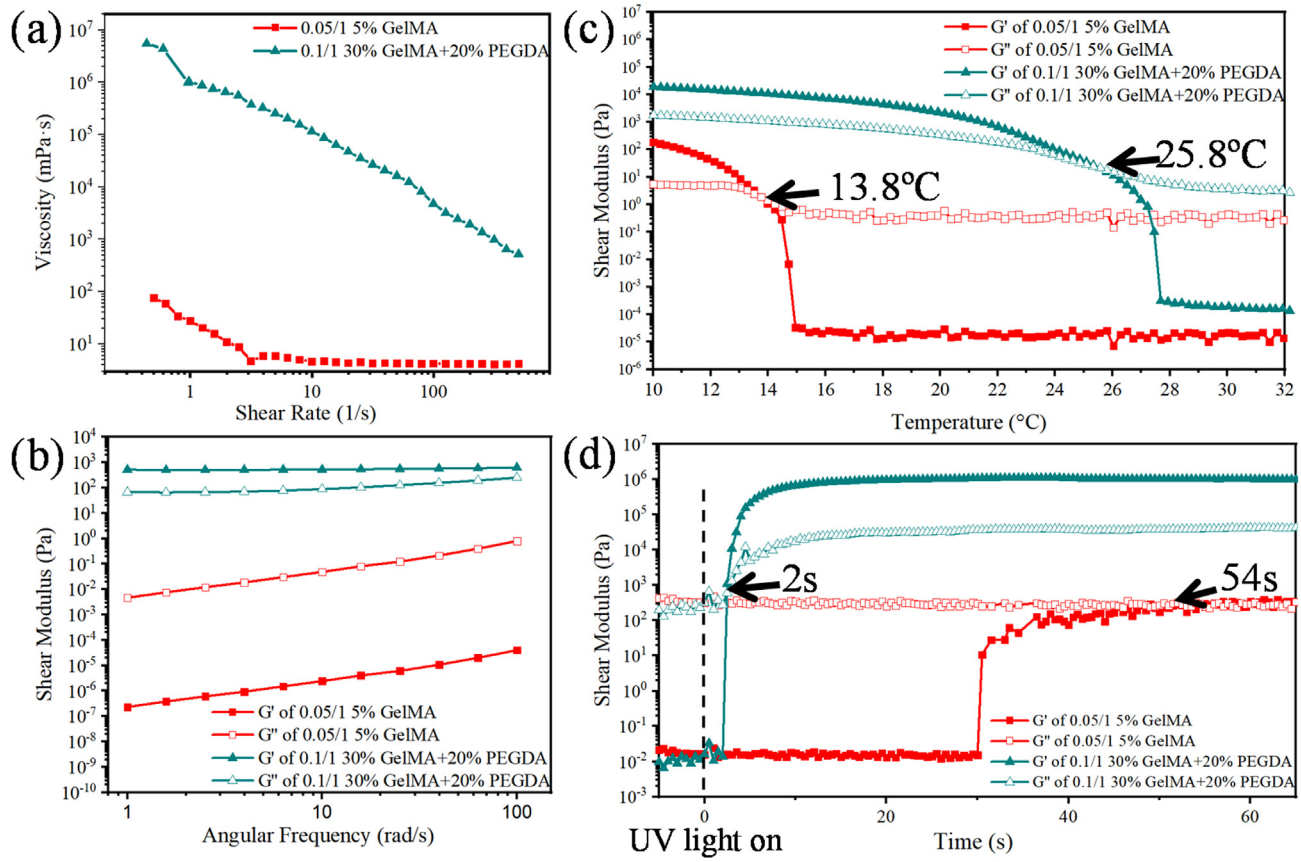


**Fig. 6.** Rheological analysis for GelMA/PEGDA hydrogels. (a) Rotational shear-viscosity measurements. (b), (c) Frequency and temperature dependence of shortage (*G′*) and loss moduli (*G″*). (d) *In situ* rheology during UV exposure.

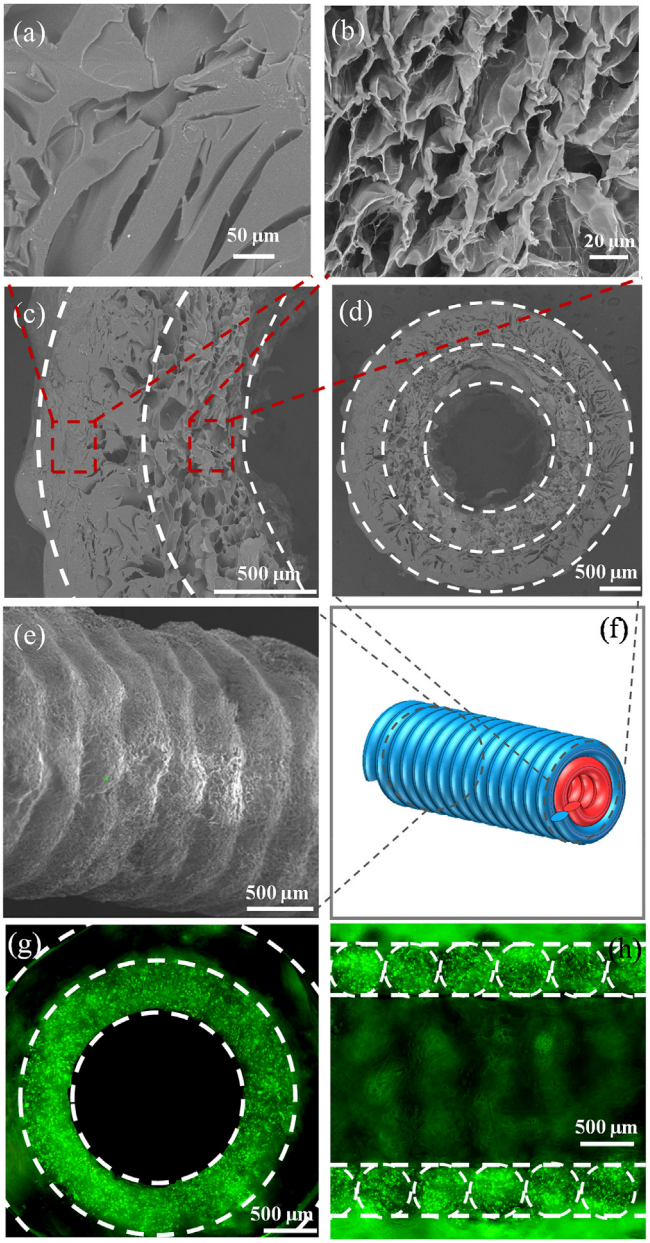


**Fig. 7.** SEM micrographs of printed nerve conduits and live/dead staining of BMSCs in the nerve conduits. The microstructure of outer layer materials (a) and inner layer materials (b) of nerve conduit. High-magnification (c) and low-magnification (d) images of nerve conduit cross-section. (e) Side view of nerve conduit outer surface. (f) Schematic of nerve conduit. Live/Dead staining for BMSCs encapsulated in nerve conduit: (g) transverse section and (h) longitudinal section.

simultaneously visualization during cells co-culture [35] (Fig. S2). The immunofluorescence staining of the PC12 cells was shown in Fig. 8a, and neurite length of PC12 cells cultured on four nerve conduits was found to increase with culture time, confirming that all groups were not cytotoxic (Fig. 8a). Compared to other groups, the neurites of PC12 cells on the nerve conduits with BMSCs were much longer after 1 day of culture (Fig. 8a). The density of PC12 cells adhered to the bilayered nerve conduits with BMSCs was much larger than on the other groups (Fig. 8b). Biocompatibility of the acellular bilayered nerve conduit was found to be comparable with single-layered 0.05/1 5% (w/v) GelMA-based nerve conduit, which was better than 0.1/1 30% (w/v) GelMA/20% (v/v) PEGDA-based nerve conduit. The proliferation rate of PC12 cells observed on the nerve conduits with BMSCs was also significantly higher than on the nerve conduits without BMSCs (Fig. 8c). Therefore, the culture of PC12 cells revealed that the addition of BMSCs into the inner layer of nerve conduits enhanced the outgrowth of PC12 cells and stimulate the PC12 cell proliferation, which indicates the co-culture of BMSCs in nerve conduits is a promising way to accelerate the regeneration of peripheral nerve.

## 4. Discussion

Biofabrication of nerve conduits has two basic biomaterial property requirements: (1) mechanical strength to resist *in vivo* physiological loads as well as facilitating the surgical operation, and (2) biocompatibility that supports appropriate behaviors of neural cells, such as cell attachment, spreading, proliferation, and differentiation. Natural material-based single-layered nerve conduits, i.e. collagen [36], chitosan [37], have excellent biocompatibility, but their weak mechanical properties limit clinical application [33]. Synthetic material-based single-layered nerve conduits, i.e. polyurethane (PU) [9,29], polyacrylonitrile (PAN) [6], poly ($_{D,\ L}$-lactide-co-glycolide) (PLGA) [38] have optimized and tunable mechanical performance, but they have poor biocompatibility and biodegradability. Therefore, our strategy to fulfill two contradictory needs was to fabricate a bilayered nerve conduit with a mechanically strong outer layer and biological inner layer. Here, a multi-nozzle additive-lathe 3D bioprinting provided a reliable method to form integrated GelMA/PEGDA bilayered nerve conduits. SEM images demonstrated the inner and outer layers were seamlessly integrated (Fig. 7), which effectually eliminated inner layer collapse and blockage of the nerve conduit lumen.

Recently, cell-based therapy has shown great promise for conduit-mediated nerve regeneration. This therapy introduces supportive cells, a biological cue, to nerve conduits, providing an appropriate microenvironment for the regenerating nerves [2]. Current cell-based protocols typically involve either cell seeding or injection into the lumen of the fabricated nerve conduits [17]. These methods generally result in cell detachment or leakage after the implantation of nerve conduits. Here, BMSCs were incorporated into the inner layer of bilayered nerve conduits through a multi-nozzle additive-lathe 3D bioprinting. This biomanufacturing technique not only avoids cell detachment or leakage, but also enables the control of cellular spatial distribution and density. Based on the results of immunofluorescent staining and CCK-8 tests of PC12 outgrowth (Fig. 8), BMSCs embedded in nerve conduits significantly enhanced the outgrowth of PC12 cell neurites and stimulated the PC12 cells proliferation. These results indicate that of BMSCs embedded nerve conduits can potentially accelerate nerve regeneration.

GelMA was utilized as the inner layer material for cell encapsulation due to its superior biological properties [2,39]. Since the biological properties of GelMA were broadly tunable depending on DMS, as such, the optimized DMS of GelMA for cell proliferation must be determined before fabrication. The cell viability and morphology spreading of BMSCs encapsulated in GelMA hydrogels were found to be significantly improved when DMS of GelMA is reduced (Figs. 4 and 5), since the denser crosslinked network formed in GelMA hydrogels with higher DMS would heavily hamper the transportation of nutrients necessitated by cell culture and metabolites [40]. Previously, the application of low DMS GelMA required a trade-off between biological and mechanical properties, here we solved this dilemma by printing two-layer nerve conduits. The addition of PEGDA into GelMA induced a strong outer layer for mechanical support (Fig. 3).

## 5. Conclusions

In summary, a bilayered cell-encapsulated nerve conduit was constructed using additive-lathe 3D bioprinting. By optimizing bioprinting parameters, a seamlessly integrated bilayered nerve conduit was obtained, and BSMCs within the printed nerve conduits showed

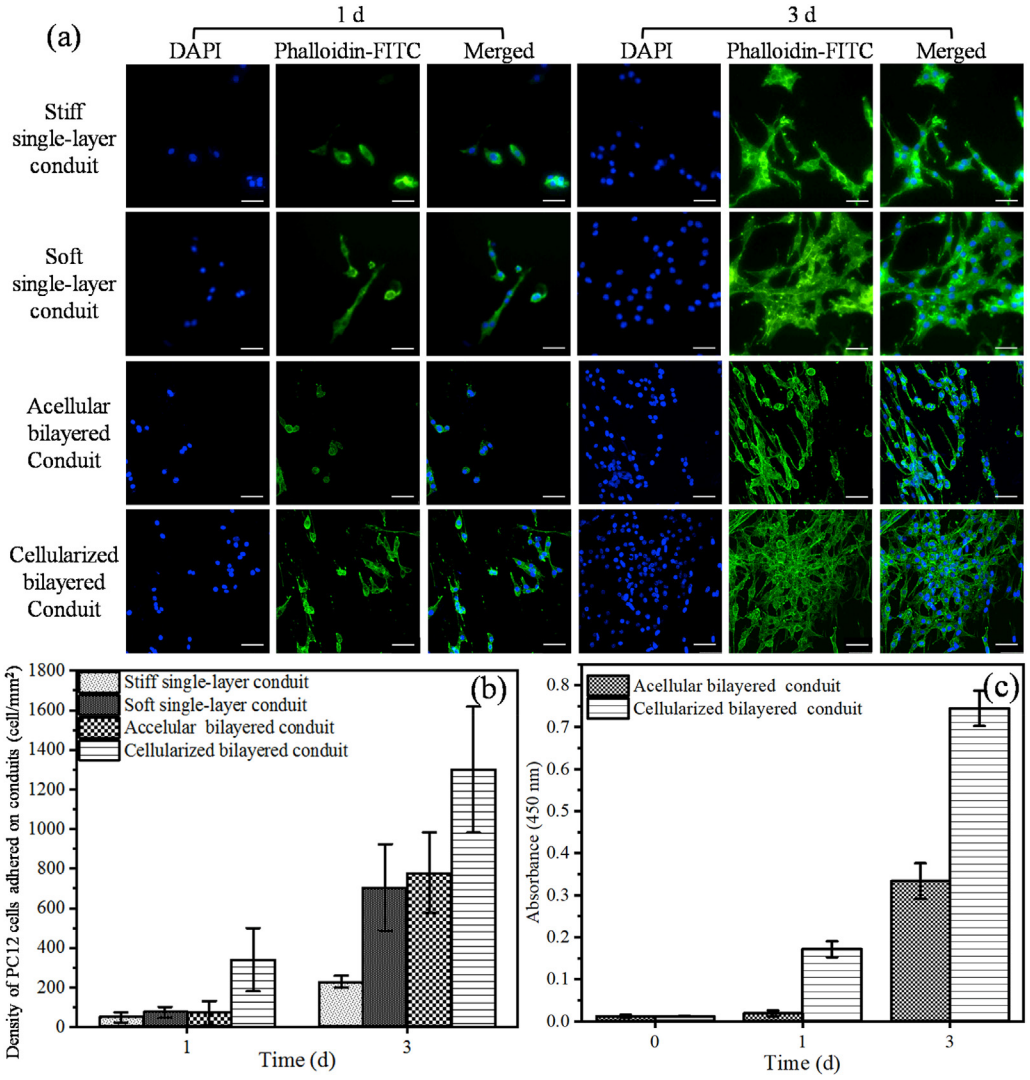


**Fig. 8.** (a) Immunofluorescence images of PC12 cells cultured on four different nerve conduits. Cell nuclei were stained by DAPI (in blue), cytoskeleton was by phalloidin-FITC (in green). (Scale bar: 50 μm) (b) The quantitative analysis of the density of PC12 cells adhered to per square millimeter of nerve conduits. (c) PC12 cell proliferation assay on acellular and cellularized bilayered nerve conduits with CCK-8 test.

exceptionally good cell viability and extended morphology. More importantly, proliferation and neurite outgrowth of PC12 cells seeded on bilayered BMSCs encapsulated nerve conduits was significantly improved compared to single-layered or acellular bilayered nerve conduits. The bilayered nerve conduit developed in this paper is a promising candidate for the repair of peripheral nerve injury.

## Author contribution

Jingyi Liu. carried out the 3D bioprinting of nerve conduits and drafted the manuscript. Bin Zhang. prepared the 3D bioprinting platform and analyzed the experimental data. Liang Li. performed in vitro cell outgrowth and revised the manuscript. Jun Yin. is the principal investigator, designed the experiments, organize and revise the manuscript. Jianzhong Fu. helped to revise the manuscript, and co-ordinate the study.

## Declaration of competing interest

The authors whose names are listed immediately below certify that they have NO affiliations with or involvement in any organization or entity with any financial interest (such as honoraria; educational grants; participation in speakers' bureaus; membership, employment, consultancies, stock ownership, or other equity interest; and expert testimony or patent-licensing arrangements), or non-financial interest (such as personal or professional relationships, affiliations, knowledge or beliefs) in the subject matter or materials discussed in this manuscript.

## Acknowledgments

This work was supported by the National Key Research and Development Program of China (Grant No. 2018YFA0703000), the Key Research and Development Program of Zhejiang Province (Grants No. 2017C01063, No. 2017C01054), the Science Fund for Creative Research Groups of the National Natural Science Foundation of China (Grant No. 51821093), and the Fundamental Research Funds for the Central Universities (Grant Nos. 2019XZZX003-02 and 2019FZA4002). The authors would like to thank Shuangshuang Liu at the Core Facility Platform of Medicine School at Zhejiang University for her technical support in confocal laser microscopy imaging.

## Appendix A. Supplementary data

Supplementary data to this article can be found online at https://doi.org/10.1016/j.bioactmat.2020.08.010.

## References


[1] J. Du, H. Chen, L. Qing, X. Yang, X. Jia, Biomimetic neural scaffolds: a crucial step towards optimal peripheral nerve regeneration, Biomaterials Science 6 (2018) 1299–1311.

[2] Y. Hu, Y. Wu, Z. Gou, J. Tao, J. Zhang, Q. Liu, T. Kang, S. Jiang, S. Huang, J. He, S. Chen, Y. Du, M. Gou, 3D-engineering of cellularized conduits for peripheral nerve regeneration, Sci. Rep. 6 (2016) 32184–32195.

[3] L. Ning, H. Sun, T. Lelong, R. Guilloteau, N. Zhu, D.J. Schreyer, X. Chen, 3D bioprinting of scaffolds with living Schwann cells for potential nerve tissue engineering applications, Biofabrication 10 (2018) 035014.

[4] Y. Qian, Q. Han, X. Zhao, J. Song, Y. Cheng, Z. Fang, Y. Ouyang, W. Yuan, C. Fan, 3D melatonin nerve scaffold reduces oxidative stress and inflammation and increases autophagy in peripheral nerve regeneration, J. Pineal Res. 65 (2018) e12516.

[5] Y. Qian, J. Song, X. Zhao, W. Chen, Y. Ouyang, W. Yuan, C. Fan, 3D fabrication with integration molding of a graphene oxide/polycaprolactone nanoscaffold for neurite regeneration and angiogenesis, Adv. Sci. 5 (2018) 1700499.

[6] J. Yin, Z. Wang, W. Chai, G. Dai, H. Suo, N. Zhang, X. Wen, Y. Huang, Fabrication of inner grooved hollow fiber membranes using microstructured spinneret for nerve regeneration, J. Manuf. Sci. Eng. 139 (2017) 111007.

[7] H. Suo, Z. Wang, G. Dai, J. Fu, J. Yin, L. Chang, Polyacrylonitrile nerve conduits with inner longitudinal grooved textures to enhance neuron directional outgrowth, Journal of Microelectromechanical Systems 27 (2018) 457–463.

[8] X. Gu, F. Ding, Y. Yang, J. Liu, Construction of tissue engineered nerve grafts and their application in peripheral nerve regeneration, Prog. Neurobiol. 93 (2011) 204–230.

[9] J. Yin, D. Zhang, Y. Xiang, P. Wei, Z. Yang, Z. Wang, J. Fu, The influence of cross-sectional morphology on the compressive resistance of polymeric nerve conduits, Polymer 148 (2018) 93–100.

[10] S. Hsu, W. Kuo, Y. Chen, C. Yen, Y. Chen, K. Chen, W. Huang, H. Cheng, New nerve regeneration strategy combining laminin-coated chitosan conduits and stem cell therapy, Acta Biomater. 9 (2013) 6606–6615.

[11] N. Golafshan, H. Gharibi, M. Kharaziha, M. Fathi, A facile one-step strategy for development of a double network fibrous scaffold for nerve tissue engineering, Biofabrication 9 (2017) 025008.

[12] L. Ning, H. Sun, T. Lelong, R. Guilloteau, N. Zhu, D.J. Schreyer, X. Chen, 3D bioprinting of scaffolds with living Schwann cells for potential nerve tissue engineering applications, Biofabrication 10 (2018) 035014.

[13] L. Ning, N. Zhu, F. Mohabatpour, M.D. Sarker, D.J. Schreyer, X. Chen, Bioprinting Schwann cell-laden scaffolds from low-viscosity hydrogel compositions, J. Mater. Chem. B 7 (2019) 4538–4551.

[14] Q. Zhang, P.D. Nguyen, S. Shi, J.C. Burrell, D.K. Cullen, A.D. Le, 3D bio-printed scafold-free nerve constructs with human gingivaderived mesenchymal stem cells promote rat facial nerve regeneration, Sci. Rep. 8 (2018) 6634.

[15] Y. Cui, Y. Yao, Y. Zhao, Z. Xiao, Z. Cao, S. Han, X. Li, Y. Huan, J. Pan, J. Dai, Functional collagen conduits combined with human mesenchymal stem cells promote regeneration after sciatic nerve transection in dogs, Journal of Tissue Engineering and Regenerative Medicine 12 (2018) 1285–1296.

[16] H. Shi, X. Li, J. Yang, Y. Zhao, C. Xue, Y. Wang, Q. He, M. Shen, Q. Zhang, Y. Yang, F. Ding, Bone marrow-derived neural crest precursors improve nerve defect repair partially through secreted trophic factors, Stem Cell Res. Ther. 10 (2019) 397–411.

[17] A.X. Sun, T.A. Prest, J.R. Fowler, R.M. Brick, K.M. Glossa, X. Li, M. DeHart, H. Shen, G. Yang, B.N. Brown, P.G. Alexander, P.G. Tuan, Conduits harnessing spatially controlled cell-secreted neurotrophic factors improve peripheral nerve regeneration, Biomaterials 203 (2019) 86–95.

[18] N.G. Fairbairn, A.M. Meppelink, J. Ng-Glazier, M.A. Randolph, J.M. Winograd, Augmenting peripheral nerve regeneration using stem cells: a review of current opinion, World J. Stem Cell. 7 (2015) 11–26.

[19] B.D. Fairbanks, M.P. Schwartz, C.N. Bowman, K.S. Anseth, Photoinitiated polymerization of PEG-diacrylate with lithium phenyl-2,4,6-trimethylbenzoylphosphinate: polymerization rate and cytocompatibility, Biomaterials 30 (2009) 6702–6707.

[20] J. Yin, M. Yan, Y. Wang, J. Fu, H. Suo, 3D bioprinting of low-concentration cell-laden gelatin methacrylate (GelMA) bioinks with a two-step cross-linking strategy, ACS Appl. Mater. Interfaces 10 (2018) 6849–6857.

[21] J. Liu, L. Li, H. Suo, M. Yan, J. Yi, J. Fu, 3D printing of biomimetic multi-layered GelMA/nHA scaffold for osteochondral defect repair, Mater. Des. 171 (C) (2019) 107708.

[22] Z. Wang, Z. Tian, F. Menard, K. Kim, Comparative study of gelatin methacrylate hydrogels from different sources for biofabrication applications, Biofabrication 9 (2017) 044101.

[23] X. Zhang, J. Li, P. Ye, G. Gao, K. Hubbell, X. Cui, Coculture of mesenchymal stem cells and endothelial cells enhances host tissue integration and epidermis maturation through AKT activation in gelatin methacryloyl hydrogel-based skin model, Acta Biomater. 59 (2017) 317–326.

[24] A. Lueckgen, D.S. Garske, A. Ellinghaus, D.J. Mooney, G.N. Duda, A. Cipitria, Enzymatically-degradable alginate hydrogels promote cell spreading and in vivo tissue infiltration, Biomaterials 217 (2019) 119294.

[25] P. Kim, A. Yuan, K.H. Nam, A. Jiao, D.H. Kim, Fabrication of poly(ethylene glycol): gelatin methacrylate composite nanostructures with tunable stiffness and degradation for vascular tissue engineering, Biofabrication 6 (2014) 024112.

[26] S.H. Kim, Y.K. Yeon, J.M. Lee, J.R. Chao, Y.J. Lee, Y.B. Seo, M.T. Sultan, O.J. Lee, J.S. Lee, S. Yoon, I. Hong, G. Khang, S.J. Lee, J.J. Yoo, C.H. Park, Precisely printable and biocompatible silk fibroin bioink for digital light processing 3D printing, Nat. Commun. 9 (2018) 1620–1633.

[27] I. Holland, J. Logan, J. Shi, C. McCormick, D. Liu, W. Shu, 3D biofabrication for tubular tissue engineering, Bio-Design and Manufacturing 1 (2018) 89–100.

[28] H. Liu, H. Zhou, H. Lan, T. Liu, X. Liu, H. Yu, 3D printing of artificial blood vessel: study on multi-parameter optimization design for vascular molding effect in alginate and gelatin, Micromachines 8 (2017) 237–246.

[29] Z. Wang, J. Lin, D. Zhang, B. Xun, J. Yin, J. Qian, G. Dai, N. Zhang, X. Wen, Y. Huang, J. Fu, Porous morphology and mechanical properties of poly(lactide-co-glycolide) hollow fiber membranes governed by ternary-phase inversion, J. Membr. Sci. 579 (2019) 180–189.

[30] A. Singh, P.A. Shiekh, M. Das, J. Seppälä, A. Kumar, Aligned chitosan-gelatin cryogel-filled polyurethane nerve guidance channel for neural tissue engineering: fabrication, characterization, and in vitro evaluation, Biomacromolecules 20 (2019) 662–673.

[31] A. Lueckgen, D.S. Garske, A. Ellinghaus, D.J. Mooney, G.N. Duda, A. Cipitria, Enzymatically-degradable alginate hydrogels promote cell spreading and in vivo tissue infiltration, Biomaterials 217 (2019) 119294.

[32] Hu, Y.; Wu, Y.; Gou, Z.; Tao, J.; Zhang, J.; Liu, Q.; Kang, T.; Jiang, S.; Huang, S.; He, J.; Chen, S.; Du, Y.; Gou, M. 3D-engineering of cellularized conduits for peripheral nerve regeneration. Sci. Rep., 6, 32184.

[33] A.R. Dixona, S.H. Jariwala, Z. Bilis, J.R. Loverde, P.F. Pasquina, L.M. Alvarez, Bridging the gap in peripheral nerve repair with 3D printed and bioprinted conduits, Biomaterials 186 (2018) 44–63.

[34] W. Zhu, K.R. Tringale, S.A. Woller, S. You, S. Johnson, H. Shen, J. Schimelman, M. Whitney, J. Steinauer, W. Xu, T.L. Yaksh, Q.T. Nguyen, S. Chen, Rapid continuous 3D printing of customizable peripheral nerve guidance conduits, Mater. Today 21 (2018) 951–959.

[35] W. Shi, B. Hass, M.A. Kuss, H. Zhang, S. Ryu, D. Zhang, T. Li, Y. Li, B. Duan, Fabrication of versatile dynamic hyaluronic acid-based hydrogels, Carbohydr. Polym. 233 (2020) 115803.

[36] S. Madduri, K. Feldman, T. Tervoort, M. Papaloïzos, B. Gander, Collagen nerve conduits releasing the neurotrophic factors GDNF and NGF, J. Contr. Release 143 (2010) 168–174.

[37] A. Wang, Q. Ao, W. Cao, M. Yu, Q. He, L. Kong, L. Zhang, Y. Gong, X. Zhang, Porous chitosan tubular scaffolds with knitted outer wall and controllable inner structure for nerve tissue engineering, J. Biomed. Mater. Res. 79A (2006) 36–46.

[38] N. Zhang, C. Zhang, X. Wen, Fabrication of semipermeable hollow fiber membranes with highly aligned texture for nerve guidance, J. Biomed. Mater. Res. 75A (2005) 941–949.

[39] Z. Jiang, H. Wang, K. Yu, Y. Feng, Y. Wang, T. Huang, K. Lai, Y. Xi, G. Yang, Light-controlled BMSC sheet–implant complexes with improved osteogenesis via an LRP5/β-catenin/runx2 regulatory loop, ACS Appl. Mater. Interfaces 9 (2017) 34674–34686.

[40] B.J. Klotz, D. Gawlitta, A.J.W.P. Rosenberg, J. Malda, F.P.W. Melchels, Gelatin-methacryloyl hydrogels: towards biofabrication-based tissue repair, Trends Biotechnol. 34 (2016) 394–407.